*Electronic Supplementary Information (ESI)*

# Porous N-doped carbon with confined Fe doped CoP grown on CNTs for superefficient oxygen evolution electrocatalysis

Manman Guo,[*a] Yuxi Yuan,[a] Yaohui Qu,[a] Ting Yu,[*a] Cailei Yuan,[a] and Zhang-hui Lu[b]

[a] *Jiangxi Key Laboratory of Nanomaterials and Sensors, School of Physics, Communication and Electronics, Jiangxi Normal University, Nanchang 330022, People's Republic of China*

[b] *College of Chemistry and Chemical Engineering, Jiangxi Normal University, Nanchang 330022, People's Republic of China*

[*] Corresponding author. Tel./fax: +86-791-88120370

*E-mail addresses:* guomanman@jxnu.edu.cn (M. Guo); yuting2014@jxnu.edu.cn (T. Yu).

**Experimental**

***Reagents***: Polyvinyl pyrrolidone (PVP, K30), $Co(NO_3)_2 \cdot 6H_2O$, $Zn(NO_3)_2 \cdot 6H_2O$, 2-methylimidazole (2-mim), $K_3[Fe(CN)_6]$, methanol, alcohol, $NaH_2PO_2 \cdot H_2O$ and KOH were of analytical grade and purchased from Sinopharm Chemical Reagent Co. Ltd., while the commercial $RuO_2$ catalyst and 5 wt % Nafion solution from Sigma-Aldrich. Carboxylic multiwall CNTs (purity $\geq$ 95%, diameter: 10–20 nm, length: 10–30 μm) were obtained from Suzhou Hengqiu technology Co. Ltd. Ultrapure water was prepared with the Millipore system and used throughout all experiments.

***Synthesis of the ZIFs/CNTs***: 20 mg CNTs and 200 mg of PVP were first sonicated in 8 mL water/methanol mixed solvent ($V_{water}:V_{methanol}$ = 1:4) for 1 h and then denoted as solution A. 0.366 g mixed metal salt ($Zn(NO_3)_2:6H_2O/Co(NO_3)_2:6H_2O$ with the mass ratio of 5:5) and 0.811 g 2-mim were ultrasonically dissolved in 12 mL and 20 mL of methanol, denoted as solution B and solution C, respectively. Solution B was quickly poured into the solution C, stirred for 10 s to obtain a clear purple solution, and then solution A was added. After stirred for 180 min, the ZIFs/CNTs products were centrifuged and washed with methanol solvent for three times, redispersed in the 20 mL water and freeze-dried for 24 h. For comparison, ZIFs were synthesized without the addition of CNTs solution.

***Synthesis of the ZIFs@PBA/CNTs***: 40 mg ZIFs/CNTs and 20 mg $K_3[Fe(CN)_6]$ were ultrasonically dispersed in 36 mL ethanol and 4 mL $H_2O$, respectively. Then the $K_3[Fe(CN)_6]$ aqueous solution was injected into ZIFs/CNTs ethanol solution and continuously stirred for 2 h. After centrifuged and washed by ethanol and ultrapure water for three times, the six parallel

as-prepared ZIFs@PBA/CNTs products were redispersed in the 20 mL water and freeze-dried for 24 h. Similarly, ZIFs@PBA were prepared by using ZIFs.

***Synthesis of the Fe-Co@PNC/CNTs***: 120 mg ZIFs@PBA/CNTs powder was placed in a corundum boat with a lid, heated to 800 °C with a heating rate of 5 °C min$^{-1}$ and maintained for 180 min under Ar atmosphere. After naturally cooled down to room temperature, the obtained sample was Fe-Co@PNC/CNTs. According to the same procedure of heating treatment, Co@PNC/CNTs and Fe-Co@PNC were also prepared with ZIFs/CNTs and ZIFs@PBA, respectively. Fe-Co$_3$O$_4$ nanoparticles (NPs) were obtained by heating Fe-Co@PNC in a muffle furnace at 450 ºC for 360 min.

***Synthesis of the Fe-CoP@PNC/CNTs***: Before in situ phosphorization, 50 mg Fe-Co@PNC/CNTs powder was pre-oxidized in a heated muffle furnace at 350 ºC for 10 min. Then the powder was further phosphatized in the quartz tube furnace by heating the upstream NaH$_2$PO$_2$·H$_2$O crystals to 350 °C with a rate of 2 °C min$^{-1}$ and maintained for 120 min under Ar atmosphere. The mass ratio of NaH$_2$PO$_2$·H$_2$O and powder was 20:1. The obtained black powder was denoted as Fe-CoP@PNC/CNTs. For comparison, CoP@PNC/CNTs, Fe-CoP@PNC and Fe-CoP NPs were also obtained under the same preparation with Co@PNC/CNTs, Fe-Co@PNC and Fe-Co$_3$O$_4$ NPs, respectively.

***Materials characterization:*** Morphology and structure of the samples were characterized with a field-emission scanning electron microscopy (SEM, Carl ZEISS, Merlin Compact) and a transmission electron microscopy (TEM, JEOL, JEM-2100). X-ray diffraction (XRD) patterns were acquired using a powder X-ray diffractometer (PANalytical B.V., X`Pert3

Powder). The nitrogen adsorption/desorption isotherms and pore-size distribution were determined by a surface area and pore size analyzer (Japan BEL, BELSORP-mini II). The Raman spectra were recorded on a laser micro-Raman spectrometer (HORIBA Scientific, HR Evolution). The chemical state and electron interaction of samples were measured by X-ray photoelectron spectroscopy (XPS, Shimadzu, AXIS Supra).

***Electrochemical measurement:*** All electrochemical measurements were performed in 1 M KOH aqueous solution by using a CHI760E electrochemical workstation (Chenhua Instruments, Shanghai, China). A typical three-electrode configuration was adopted with a catalyst-modified glass carbon electrode (GCE, 3 mm in diameter), a graphite rod and a saturated calomel electrode (SCE) as working, counter and reference electrodes, respectively. The working electrode was modified by the following processes: 5 mg catalyst powder was added in a mixed solution of 960 μL ethanol and 40 μL nafion 5 wt % Nafion solution and ultrasonicated for 30 min to form a homogeneous catalyst ink. Then, 8 μL ink was droped on the GCE (with the mass loading of 0.566 mg cm$^{-2}$) and dried under ambient conditions before use.

According to the Nernst equation, all potentials in this work were converted to reversible hydrogen electrode (RHE) potential without $iR_s$ compensation.[S1] Polarization curves were measured by linear sweep voltammetry (LSV) with a scanning rate of 2 mV s$^{-1}$. The Tafel curves were plotted according to the potential against log |$j$| from LSV data. Electrochemical impedance spectroscopy (EIS) was performed at overpotentials of 260 mV in a frequency range from $10^5$ to $10^{-2}$ Hz with an AC voltage of 5 mV. To evaluate the electrochemical surface area (ECSA), the double layer capacitance ($C_{dl}$) was calculated according to CV curves with

different scanning rates by plotting the capacitive currents ($\Delta j = j_{anodic} - j_{cathodic})/_2$ against the scan rates (2 to 12 mV s$^{-1}$) in the region from 1.10 to 1.20 V (vs. RHE), where no apparent Faradaic processes occurred.[S2] The ECSA and turnover frequency (TOF) can be calculated according to the following equations: ECSA = $C_{dl} \times A/(60$ μF cm$^{-2})$ and TOF = $jA/4Fm$, respectively, where $j$ is the current density,[S1] A the surface area of the electrode, F the Faraday constant (96485 C mol$^{-1}$), and m the number of moles of the active material. The catalyst durability was investigated chronopotentiometry (CP). All the electrochemical experiments were conducted at room temperature.

***DFT Calculation:*** All the DFT calculations were performed on the Vienna Ab-initio Simulation Package (VASP).[S3] The projector augmented wave (PAW) method was implanted to represent the core-electron (valence electron) interactions.[S4] The generalized gradient approximation (GGA) expressed by the Perdew-Burke-Emzerhof (PBE) functional form was employed to evaluate the electron-electron exchange and correlation interactions.[S5] The Spin-polarizations were carried out for all calculations. The energy cutoff for the plane wave basis expansion was set to 450 eV and the force on each atom less than 0.03 eV Å$^{-1}$ was set for convergence criterion of geometry relaxation. The $k$-points in the Brillouin zone were sampled by a 3× 3 × 1 grid. The self-consistent calculations apply a convergence energy threshold of 10$^{-5}$ eV. The DFT-D3 method was employed to consider the van der Waals interaction.[S6] A 15 Å vacuum was added along the z direction in order to avoid the interaction between periodic structures. The free energies of the OER steps were calculated by the equation:[S7,S8] $\Delta G = \Delta E_{DFT} + \Delta E_{ZPE} - T\Delta S$, where $\Delta E_{DFT}$ is the DFT electronic energy difference of each step, $\Delta E_{ZPE}$ and $\Delta S$ are the correction of zero-point energy and the variation of entropy, respectively, which are

obtained by vibration analysis, $T$ is the temperature (T = 300 K).
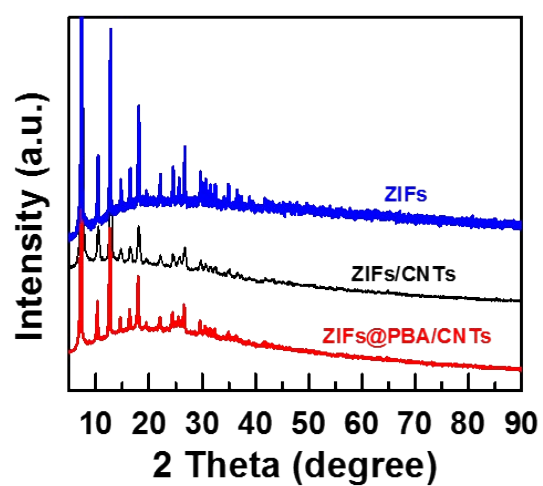


**Fig. S1** XRD patterns of ZIFs, ZIFs/CNTs and ZIFs@PBA/CNTs.
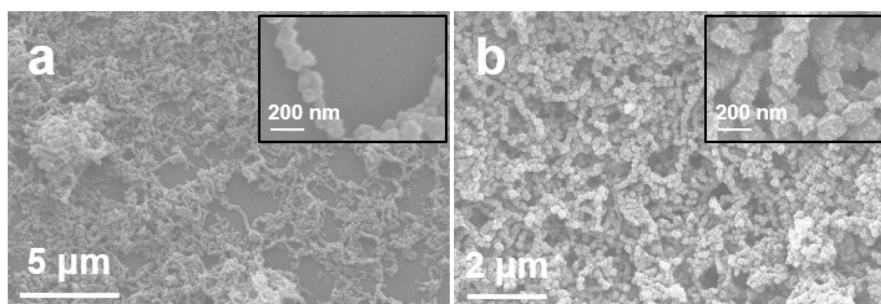


**Fig. S2** SEM images of (a) ZIFs/CNTs and (b) ZIFs@PBA/CNTs.
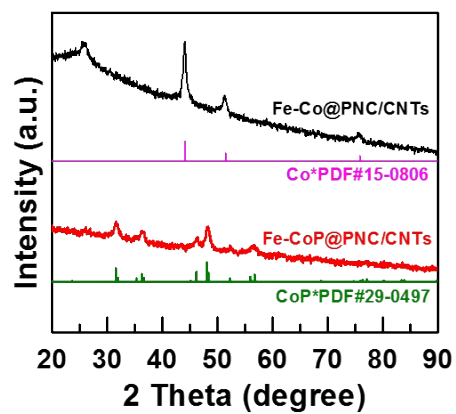
**Fig. S3** XRD patterns of Fe-Co@PNC/CNTs and Fe-CoP@PNC/CNTs.
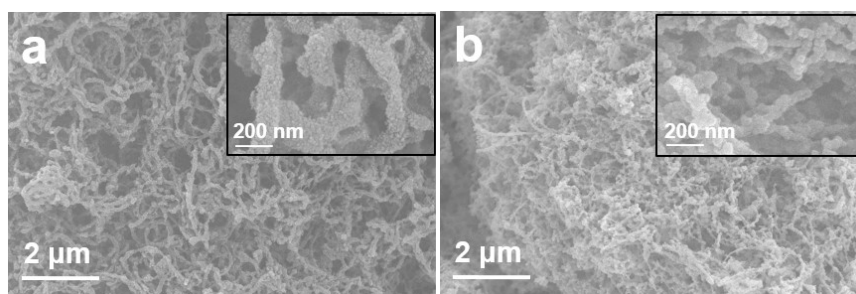


**Fig. S4** SEM images of (a) Fe-Co@PNC/CNTs and (b) Fe-CoP@PNC/CNTs.
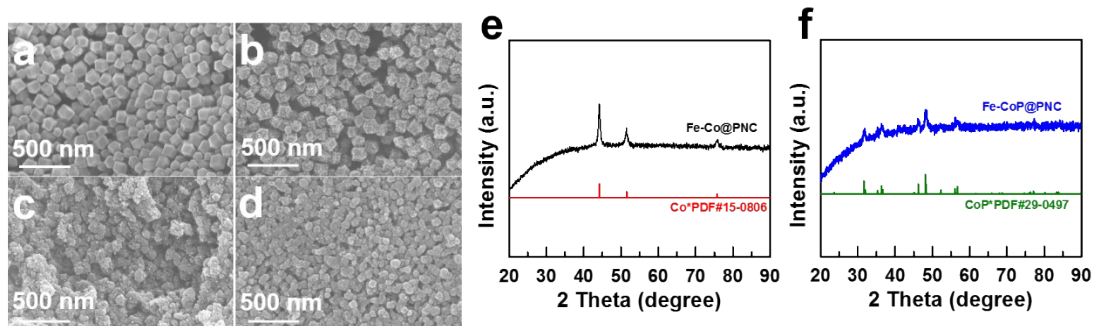
**Fig. S5** SEM images of (a) ZIFs, (b) ZIFs@PBA, (c) Fe-Co@PNC and (d) Fe-CoP@PNC. XRD patterns of (e) Fe-Co@PNC and (f) Fe-CoP@PNC.
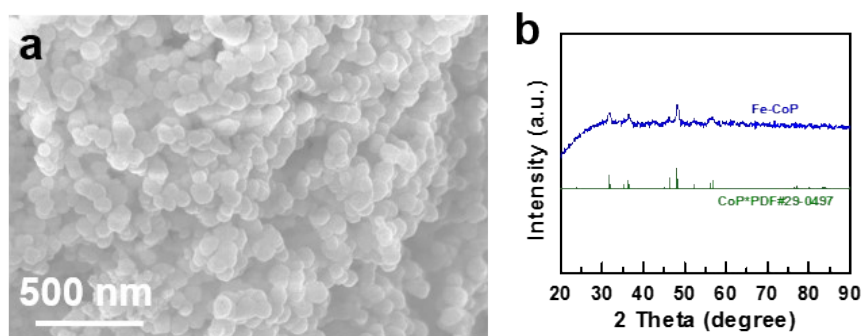


**Fig. S6** (a) SEM image and (b) XRD pattern of Fe-CoP.
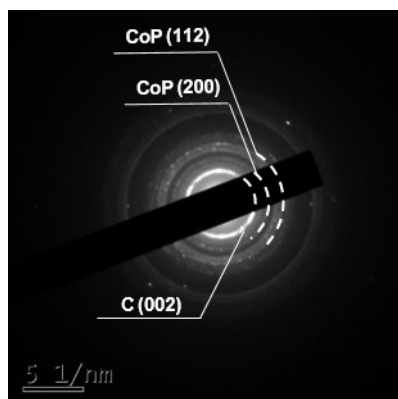
**Fig. S7** SADE pattern of Fe-CoP@PNC/CNTs.
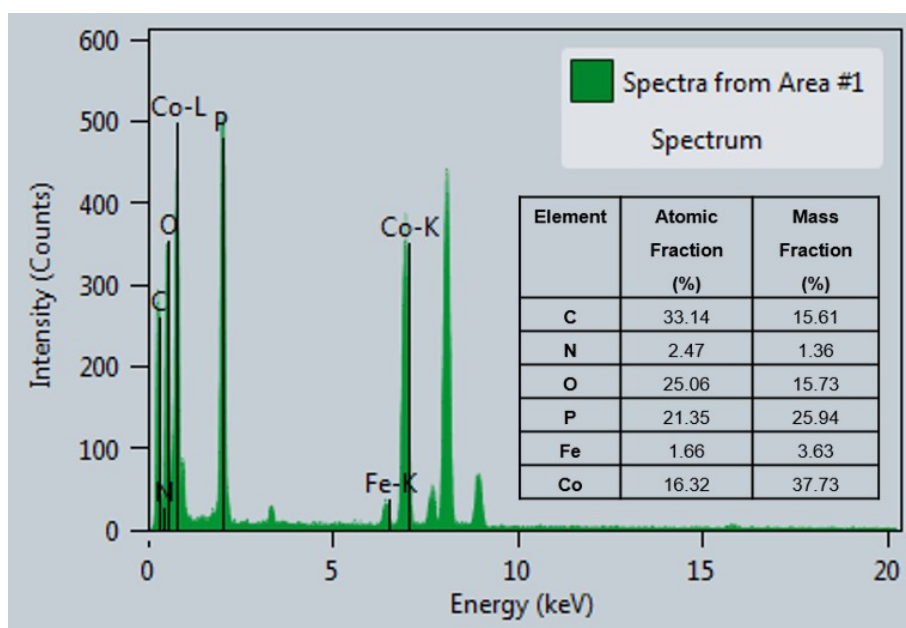


**Fig. S8** EDX spectrum of Fe-CoP@PNC/CNTs.
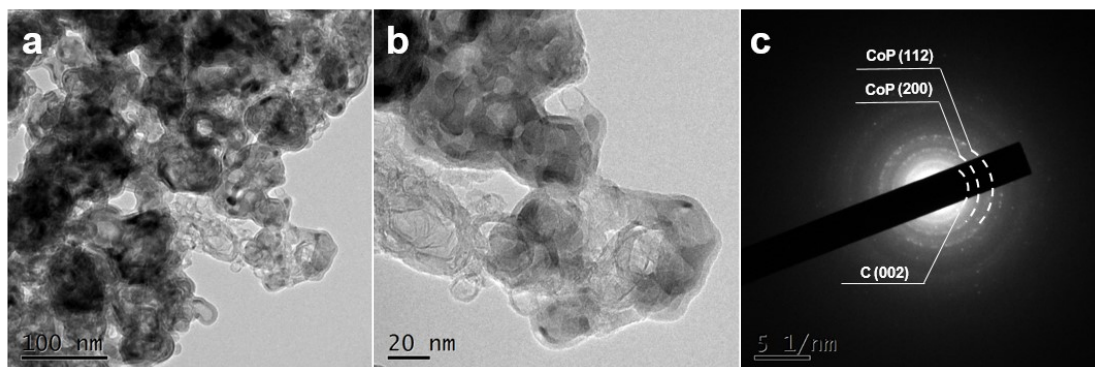
**Fig. S9** (a,b) TEM images and (c) SADE pattern of Fe-CoP@PNC.
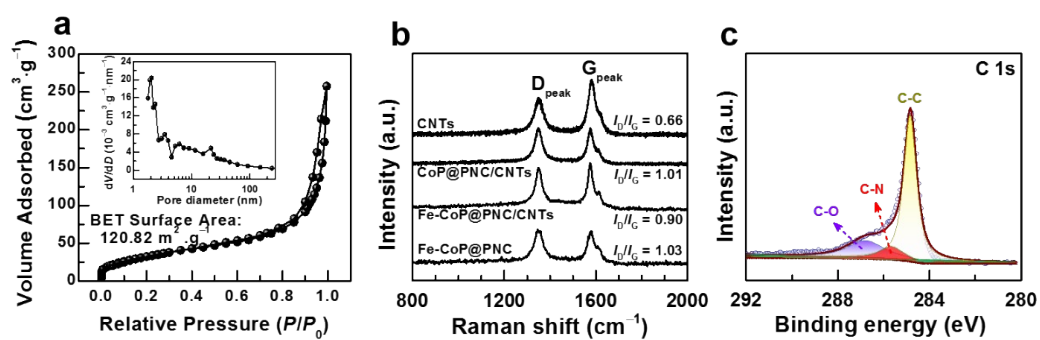


**Fig. S10** (a) $N_2$ adsorption/desorption isotherm loop and pore size distribution of Fe-CoP@PNC/CNTs. (b) Raman spectra of CNTs, CoP@PNC/CNTs, Fe-CoP@PNC/CNTs and Fe-CoP@PNC. (c) XPS high resolution C 1s spectrum of Fe-CoP@PNC/CNTs.
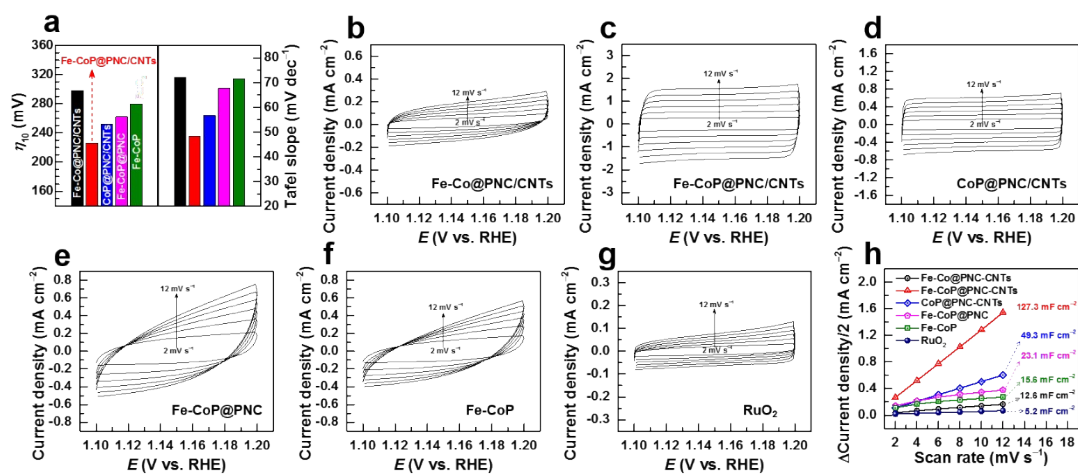
**Fig. S11** (a) Histogram of $\eta_{10}$ and Tafel slopes of the as-prepared samples. Cyclic voltammograms of (b) Fe-Co@PNC/CNTs, (c) Fe-CoP@PNC/CNTs, (d) CoP@PNC/CNTs, (e) Fe-CoP@PNC, (f) Fe-CoP and (g) RuO$_2$ in the non-faradaic region of 1.10-1.20 V vs. RHE at various scan rates in 1.0 M KOH. (h) Calculated $C_{dl}$ of the as-prepared samples and RuO$_2$.
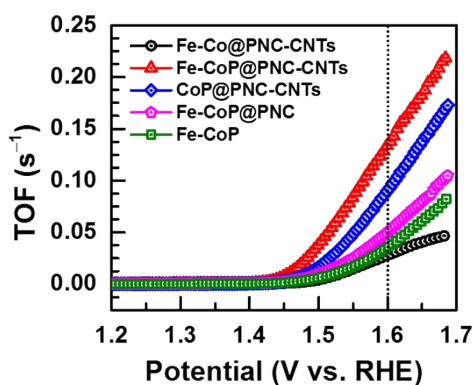


**Fig. S12** TOF curves of Fe-Co@PNC/CNTs, Fe-CoP@PNC/CNTs, CoP@PNC/CNTs, Fe-CoP@PNC and Fe-CoP in 1.0 M KOH.
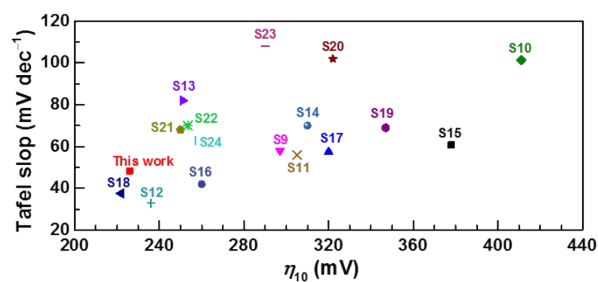
**Fig. S13** The activity comparison of Fe-CoP@PNC/CNTs with recently reported OER electrocatalysts of CoP nanorods with P vacancy,[S9] Cu-CoP nanosheets,[S10] hollow Mo-CoP nanoboxes,[S11] hollow Fe-CoP prisms,[S12] CNT-NC-CoP,[S13] CoP/NCNHP,[S14] NiCo phosphates microrods,[S15] porous (FeNiCo)OOH,[S16] P@$p$CoPc/Co$_3$O$_4$ nanosheets,[S17] core-shell CoP$_x$@FeOOH,[S18] Co(S, Se)@graphene nanofoam,[S19] porous CoP$_x$-CoO$_y$,[S20] CoO-CoSe$_2$@N-CNTs/rGO,[S21] NiCo$_2$S$_4$ microspheres/NS-rGO,[S22] Co(OH)$_2$ nanosheets@NC,[S23] S-CoTe nanorods.[S24]
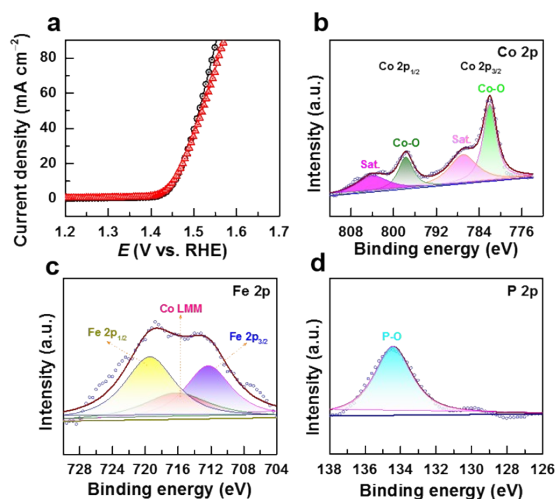


**Fig. S14** (a) Polarization curves before and after stability test of Fe-CoP@PNC/CNTs. XPS high resolution (b) Co 2p, (c) Fe 2p and (d) P 2p spectra of Fe-CoP@PNC/CNTs modified glassy carbon electrode after durability test.
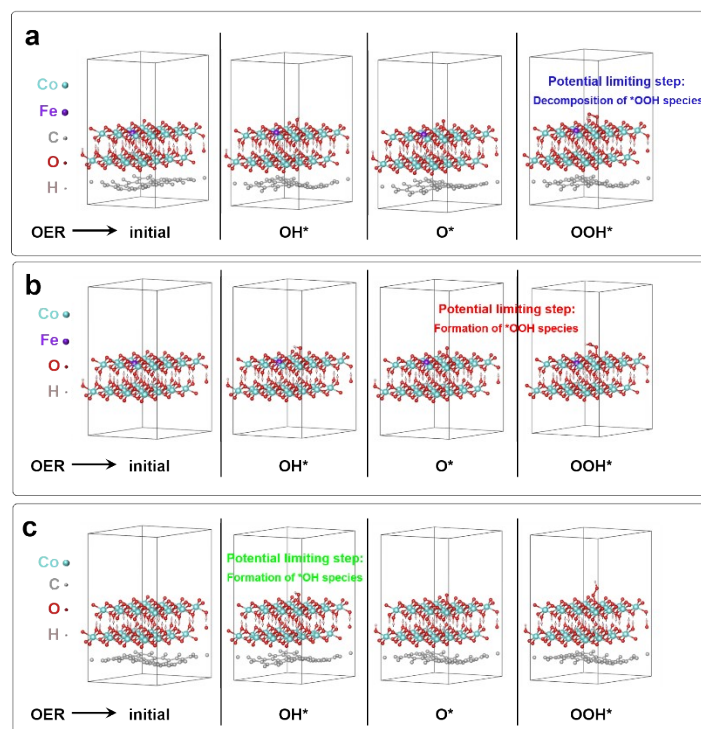
**Fig. S15** The optimized configurations of (a) Fe-CoOOH/C, (b) Fe-CoOOH and (c) CoOOH/C with

different intermediates during OER process.
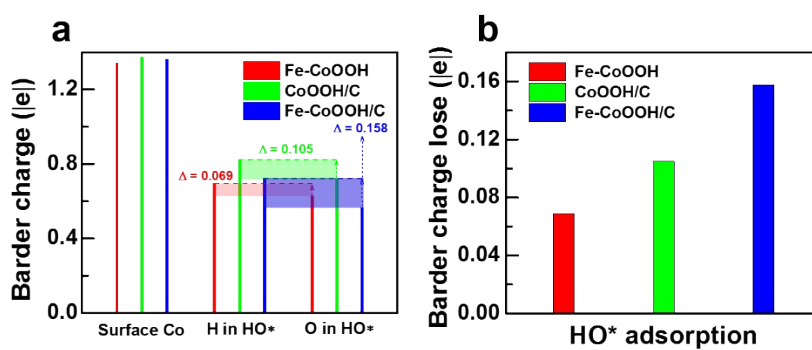


**Fig. S16** (a) Bader charge analysis for surface Co ions and H, O in HO* adsorption on Fe-CoOOH,

CoOOH/C and Fe-CoOOH/C surfaces. (b) Bader charge analysis for electron loss in HO*

adsorption on Fe-CoOOH, CoOOH/C and Fe-CoOOH/C surfaces.

**Table S1.** Comparison of OER activity of Fe-CoP@PNC/CNTs with recently reported Co-based electrocatalysts.

| No. | Catalyst | Substrate | Loading amount (mg cm$^{-2}$) | Tafel slope (mV dec$^{-1}$) | $\eta_{10}$ (mV) | Reference |
|---|---|---|---|---|---|---|
| 1 | NiCo phosphates microrods | GCE | – | 60.79 | 378 | S15 |
| 2 | Porous (FeNiCo)OOH | FeNiCo alloy sheet | – | 42 | 260 | S16 |
| 3 | P@$p$CoPc/Co$_3$O$_4$ nanosheets | CC | 0.556 | 57.4 | 320 | S17 |
| 4 | CoP nanorods with P vacancy | GCE | 0.354 | 58.1 | 297 | S9 |
| 5 | Cu-CoP nanosheets | CP | 5.17 | 101.4 | 411 | S10 |
| 6 | Core-shell CoPx@FeOOH | NF | 4.10 | 37.6 | 222 | S18 |
| 7 | CNT-NC-CoP | GCE | 0.708 | 82.1 | 251 | S13 |
| 8 | Co(S, Se)@graphene nanofoam | RDE | 0.2 | 69.0 | 347 | S19 |
| 9 | Porous CoP$_x$-CoO$_y$ | GCE | 0.2 | 102 | 322 | S20 |
| 10 | CoO-CoSe$_2$@N-CNTs/rGO | GCE | 0.28 | 68 | 250 | S21 |
| 11 | CoP/NCNHP | GCE | 0.390 | 70 | 310 | S14 |
| 12 | Hollow Fe-CoP prisms | CP | 1 | 32.9 | 236 | S12 |
| 13 | Hollow Mo-CoP nanoboxes | CC | 2.5 | 56 | 305 | S11 |
| 14 | NiCo$_2$S$_4$ microspheres/NS-rGO | NF | 0.1 | 70.1 | 253.4 | S22 |
| 15 | Co(OH)$_2$ nanosheets@NC | CC | 2.36 | 108 | 290 | S23 |

| 16 | S-CoTe nanorods | CC | – | 63 | 257 | S24 |
| 17 | Fe-CoP@PNC/CNTs | GCE | 0.566 | 48.4 | 226 | This work |

## References

S1   H. Han, K. M. Kim, J. H. Ryu, H. J. Lee, J. Woo, G. Ali, K. Y. Chung, T. Kim, S. Kang, S. Choi, J. Kwon, Y. -C. Chung, S. Mhin and T. Song, *Nano Energy*, 2020, **75**, 104945.

S2   Y. Li, B. Wei, Z. Yu, O. Bondarchuk, A. Araujo, I. Amorim, N. Zhang, J. Xu, I. C. Neves and L. Liu, *ACS Sustainable Chem. Eng.*, 2020, **8**, 10193–10200.

S3   G. Kresse and J. Hafner, *Phys. Rev. B*, 1993, **47**, 558–561.

S4   P.E. Blöchl, *Phys. Rev. B*, 1994, **50**, 17953–17979.

S5   J.P. Perdew, K. Burke and M. Ernzerhof, *Phys. Rev. Lett.*, 1996, **77**, 3865–3868.

S6   J. Harl, L. Schimka and G. Kresse, *Phys. Rev. B*, 2010, **81**, 115126.

S7   J.S. Li, Y. Wang, C.H. Liu, S.L. Li, Y.G. Wang, L.Z. Dong, Z.H. Dai, Y.F. Li and Y.Q., *Nature Commun.*, 2016, **7**, 11204.

S8   E. Skulason, T. Bligaard, S. Gudmundsdottir, F. Studt, J. Rossmeisl, F. Abild-Pedersen, T. Vegge, H. Jonsson, J.K. Norskov, *Phys. Chem. Chem. Phys.*, 2012, **14**, 1235–1245.

S9   G. Yuan, J. Bai, L. Zhang, X. Chen and L. Ren, *Appl. Catal. B-Environ.*, 2021, **284**, 119693.

S10   L. Yan, B. Zhang, J. Zhu, Y. Li, P. Tsiakaras, P. K. Shen, *Appl. Catal. B-Environ.*, 2020, **265**, 118555.

S11   C. Guan, W. Xiao, H. Wu, X. Liu, W. Zang, H. Zhang, J. Ding, Y. P. Feng, S. J. Pennycook and J. Wang, *Nano Energy*, 2018, **48**, 73–80.

S12   X. Ding, H. Huang, Q. Wan, X. Guan, Y. Fang, S. Lin, D. Chen and Z. Xie, *J. Energy Chem.*, 2021, **62**, 415–422.

S13   X. Wang, Z. Ma, L. Chai, L. Xu, Z. Zhu, Y. Hu, J. Qian and S. Huang, *Carbon*, 2019, **141**, 643–651.

S14 Y. Pan, K. Sun, S. Liu, X. Cao, K. Wu, W. -C. Cheong, Z. Chen, Y. Wang, Y. Li, Y. Liu, D. Wang, Q. Peng, C. Chen, Y. Li, *J. Am. Chem. Soc.*, 2018, **140**, 2610–2618.

S15 D. Wang, Y. Wang, Z. Fu, Y. Xu, L. -X. Yang, F. Wang, X. Guo, W. Sun, Z. -L. Yang, *ACS Appl. Mater. Interfaces*, 2021, **13**, 34507–34517.

S16 M. Nishimoto, S. Kitano, D. Kowalski, Y. Aoki and H. Habazaki, *ACS Sustainable Chem. Eng.*, 2021, **9**, 9465–9473.

S17 Y. Kim, D. Kim, J. Lee, L. Y. S. Lee and D. K. P. Ng, *Adv. Funct. Mater.*, 2021, **31**, 2103290.

S18 L. Wu, L. Yu, B. McElhenny, X. Xing, D. Luo, F. Zhang, J. Bao, S. Chen and Z. Ren. *Appl. Catal. B-Environ.*, 2021, **294**, 120256.

S19 C. Xie, Q. Wang, C. Xiao, L. Yang, M. Lan, S. Yang, J. Xiao, F. Xiao and S. Wang, *Carbon*, 2021, **178**, 640–648.

S20 H. Zhou, M. Zheng and H. Pang, *Chem. Eng. J.*, 2021, **416**, 127884.

S21 D. Xu, X. Long, J. Xiao, Z. Zhang, G. Liu, H. Tong, Z. Liu, N. Li, D. Qian, J. Li and J. Liu, *Chem. Eng. J.*, 2021, **422**, 129982.

S22 H. Li, L. Chen, P. Jin, Y. Li, J. Pang, J. Hou, S. Peng, G. Wang and Y. Shi, *Nano Res.*, **accepted, DOI:** 10.1007/s12274-021-3580-z.

S23 Y. Wang, A. Li and C. Cheng, *Small*, 2021, **17**, 2101720.

S24 L. Yang, H. Qin, Z. Dong, T. Wang, G. Wang and L. Jiao, *Small*, 2021, **17**, 2102027.